Figure01.

(a)

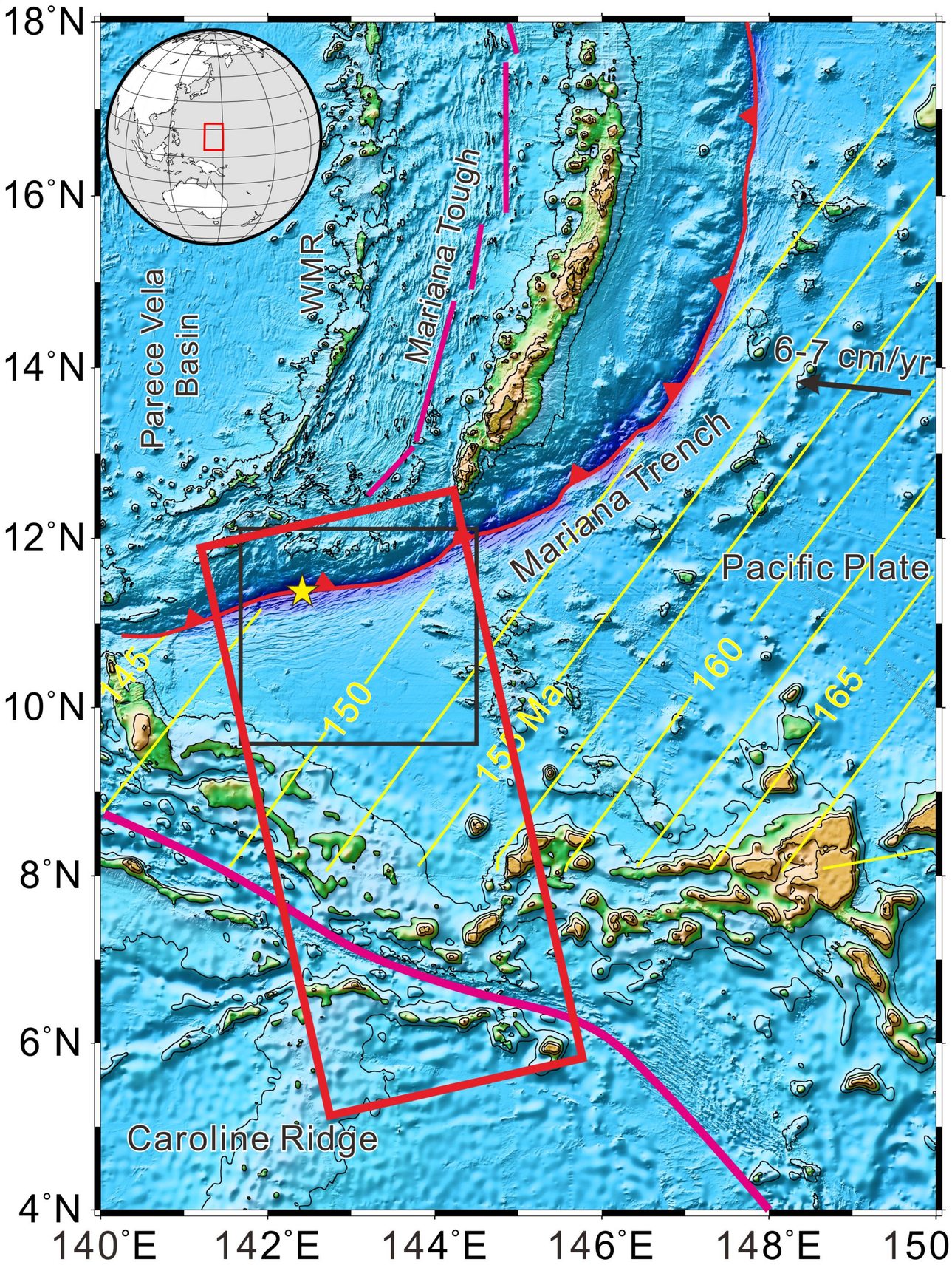
18°N
16°N
14°N
12°N
10°N
8°N
6°N
4°N
140°E
142°E
144°E
146°E
148°E
150°E
Parece Vela Basin
WMR
Mariana Tough
Mariana Trench
6-7 cm/yr
Pacific Plate
145
150
155Ma
160
165
Caroline Ridge

(b)

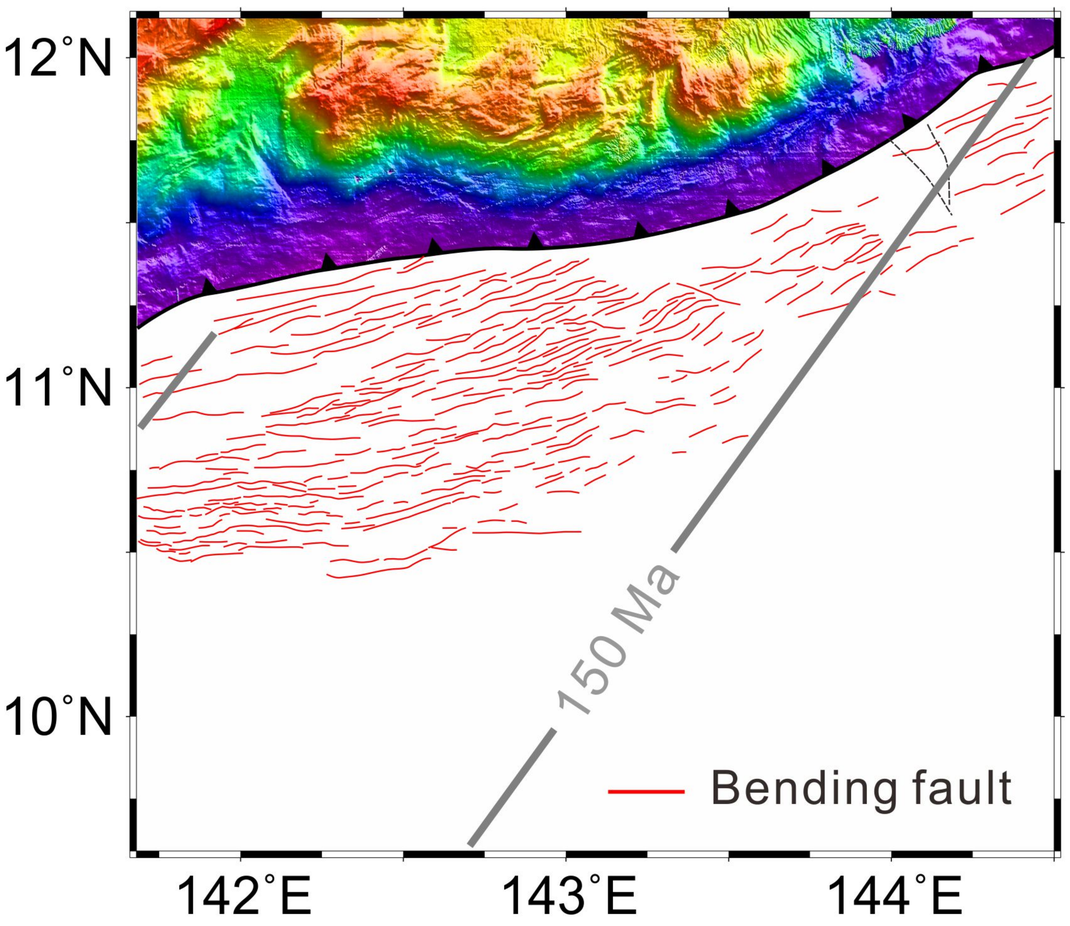
12°N
11°N
10°N
142°E
143°E
144°E
150 Ma
Bending fault

(c)

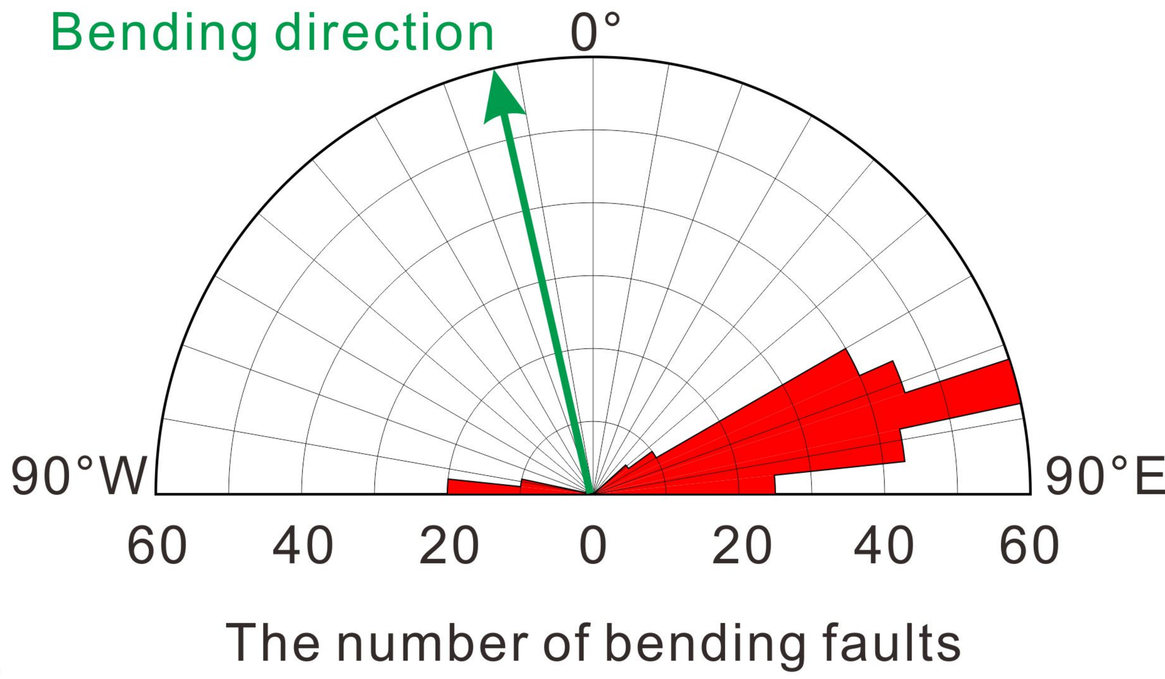
Bending direction
0°
90°W
90°E
60
40
20
0
20
40
60
The number of bending faults

(d)

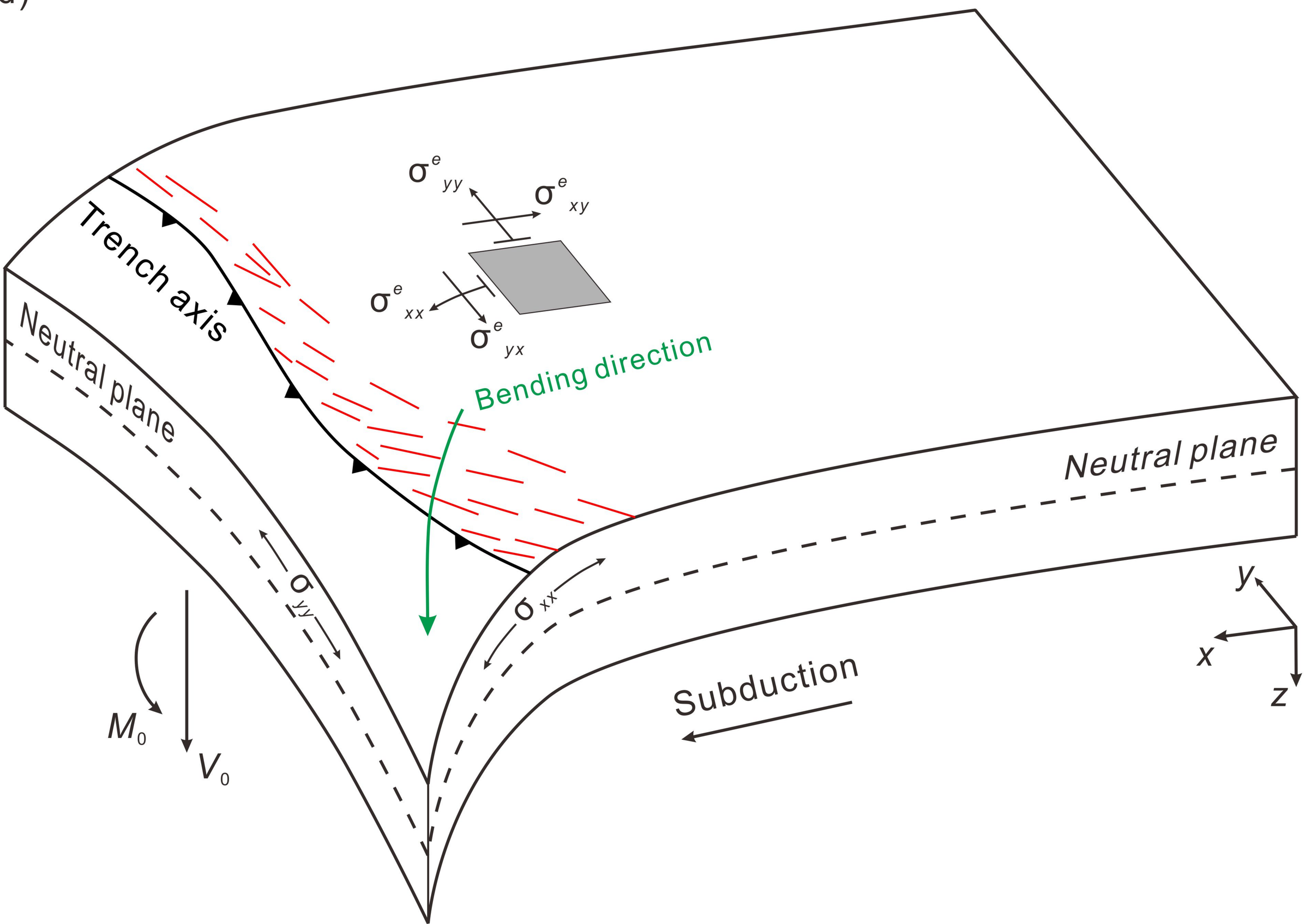
Trench axis
Neutral plane
Bending direction
Neutral plane
Subduction
y
x
z
M_0
V_0

Figure02.

a)

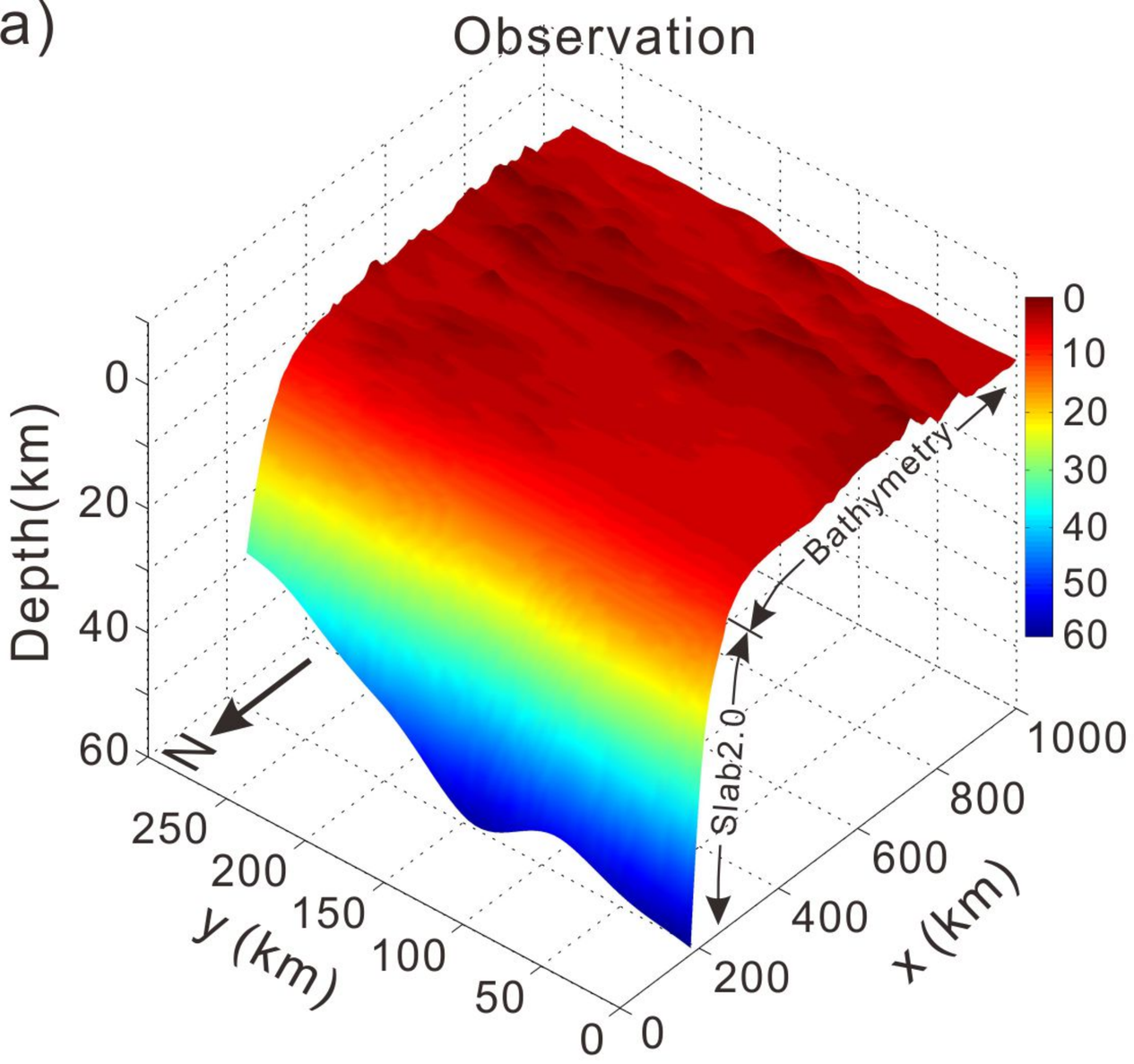
Observation
Depth(km)
0
20
40
60
N
250
200
150
100
50
0
y (km)
0
200
400
600
800
1000
x (km)
Bathymetry
Slab2.0
0
10
20
30
40
50
60

b)

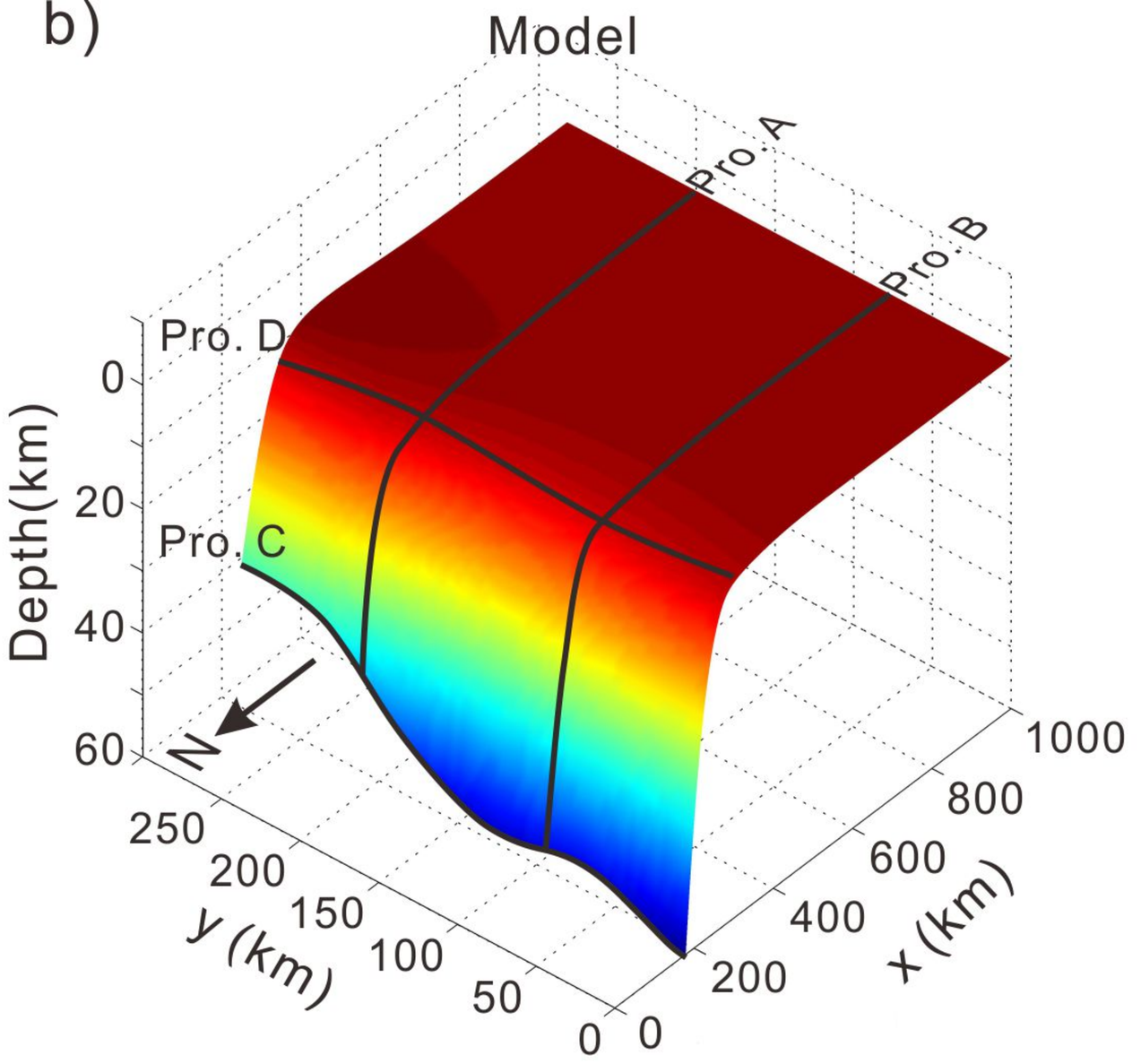
Model
Pro. A
Pro. B
Pro. D
Pro. C
Depth(km)
0
20
40
60
N
250
200
150
100
50
0
y (km)
0
200
400
600
800
1000
x (km)

c)

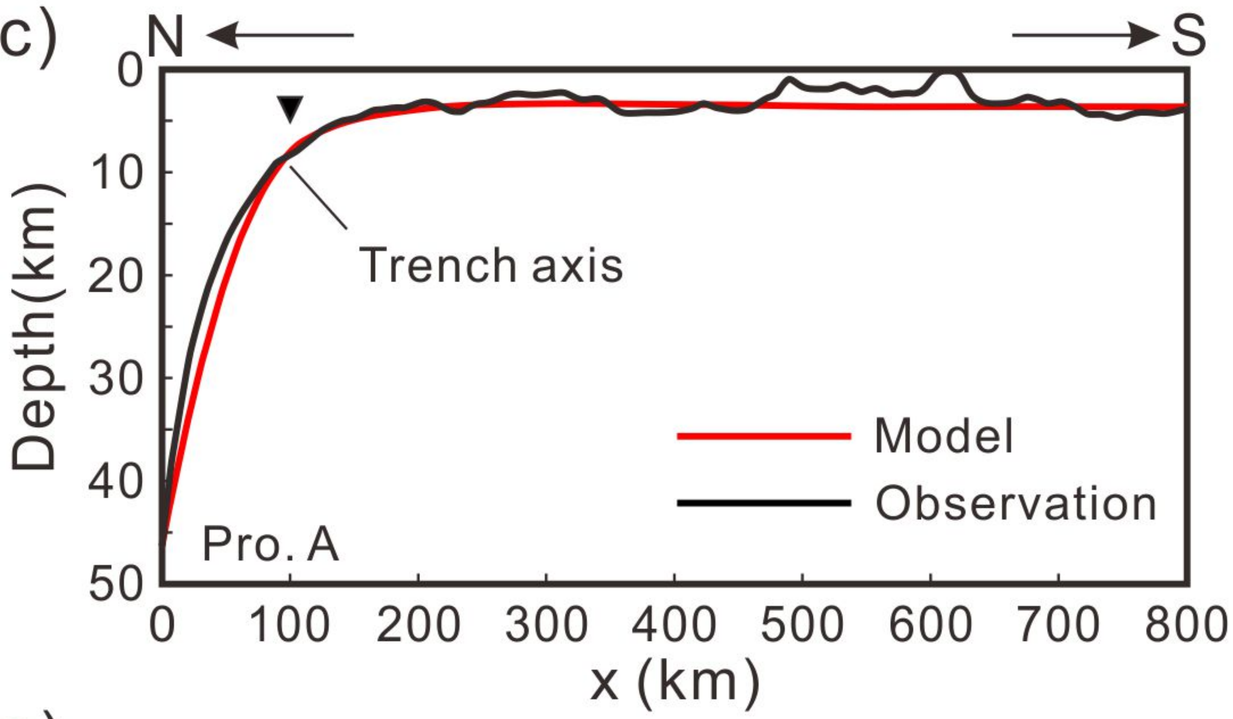
N
S
Depth(km)
0
10
20
30
40
50
Trench axis
Model
Observation
Pro. A
0
100
200
300
400
500
600
700
800
x (km)

d)

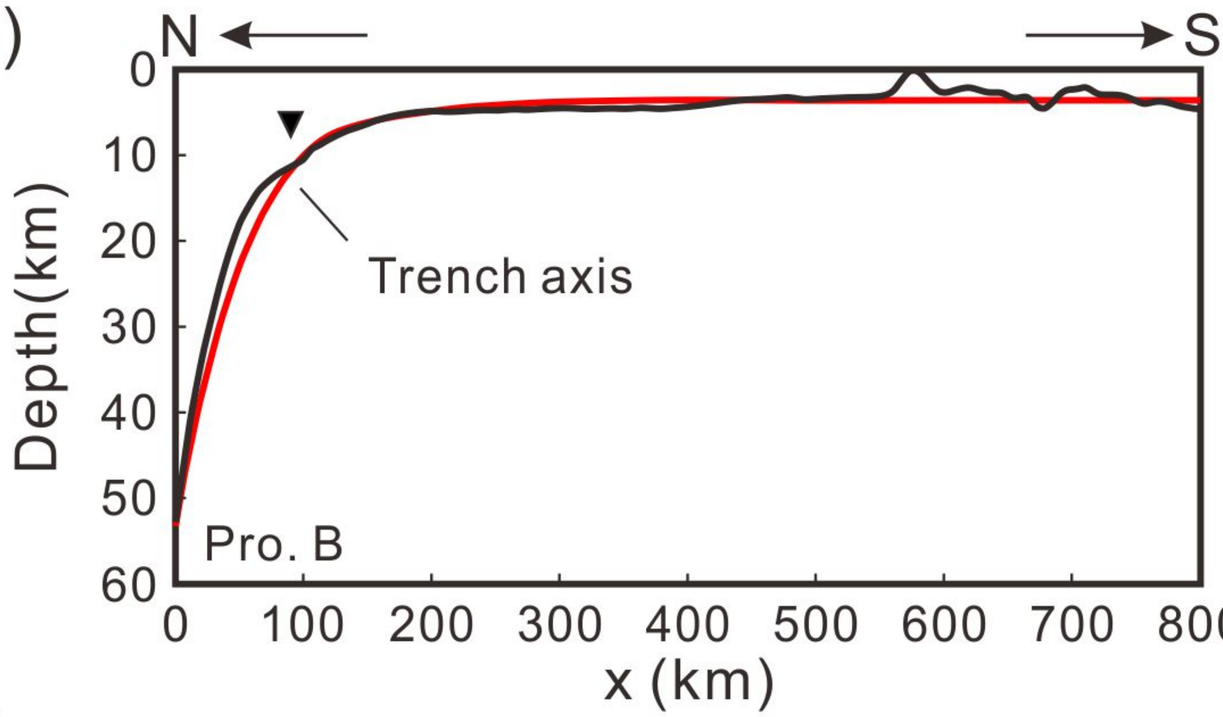
N
S
Depth(km)
0
10
20
30
40
50
60
Trench axis
Pro. B
0
100
200
300
400
500
600
700
800
x (km)

e)

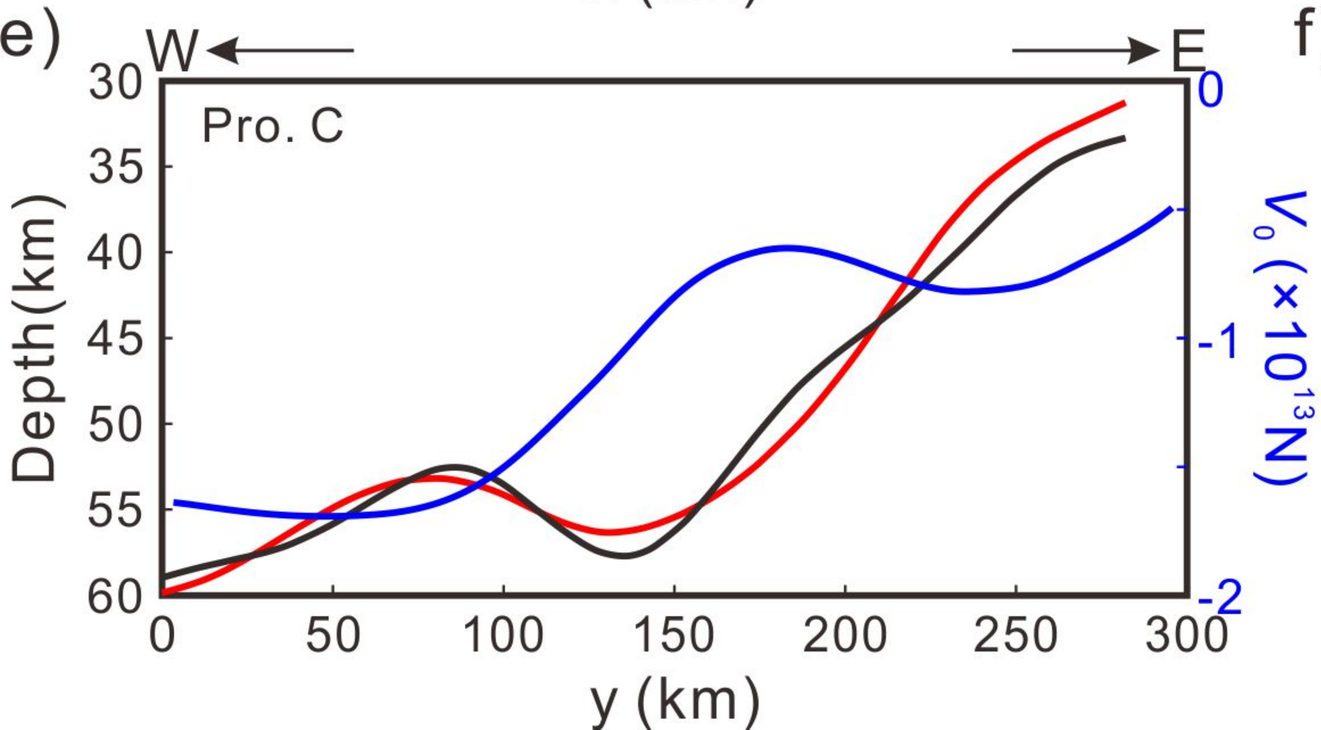
W
E
Pro. C
Depth(km)
30
35
40
45
50
55
60
0
-1
-2
V_0 ($\times 10^{13}$N)
0
50
100
150
200
250
300
y (km)

f)

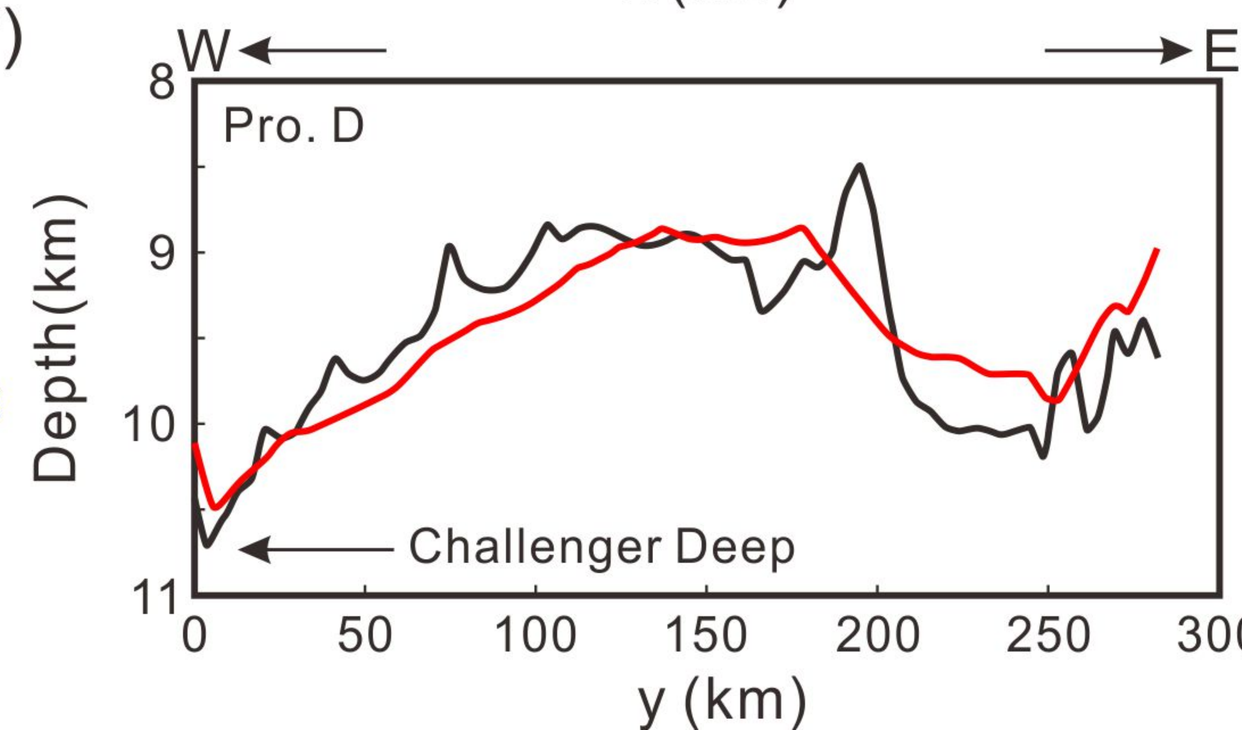
W
E
Pro. D
Depth(km)
8
9
10
11
Challenger Deep
0
50
100
150
200
250
300
y (km)

Figure03.

(a)

(b)

(c)

(d)

(e)

from Zhu et. al (2019)

from USGS

Mariana trench

Challenger Deep

σ^{e}_{xx}

σ^{e}_{yy}

σ^{e}_{xy}

σ^{e}_{1}

×10³ MPa

12°00'

11°30'

11°00'

10°30'

142°30'

143°00'

143°30'

144°00'

A

A'

W

E

Stress(×10³ MPa)

Depth (km)

Distance (km)

Seismic counts

Depth(km)

Figure04.

(a)

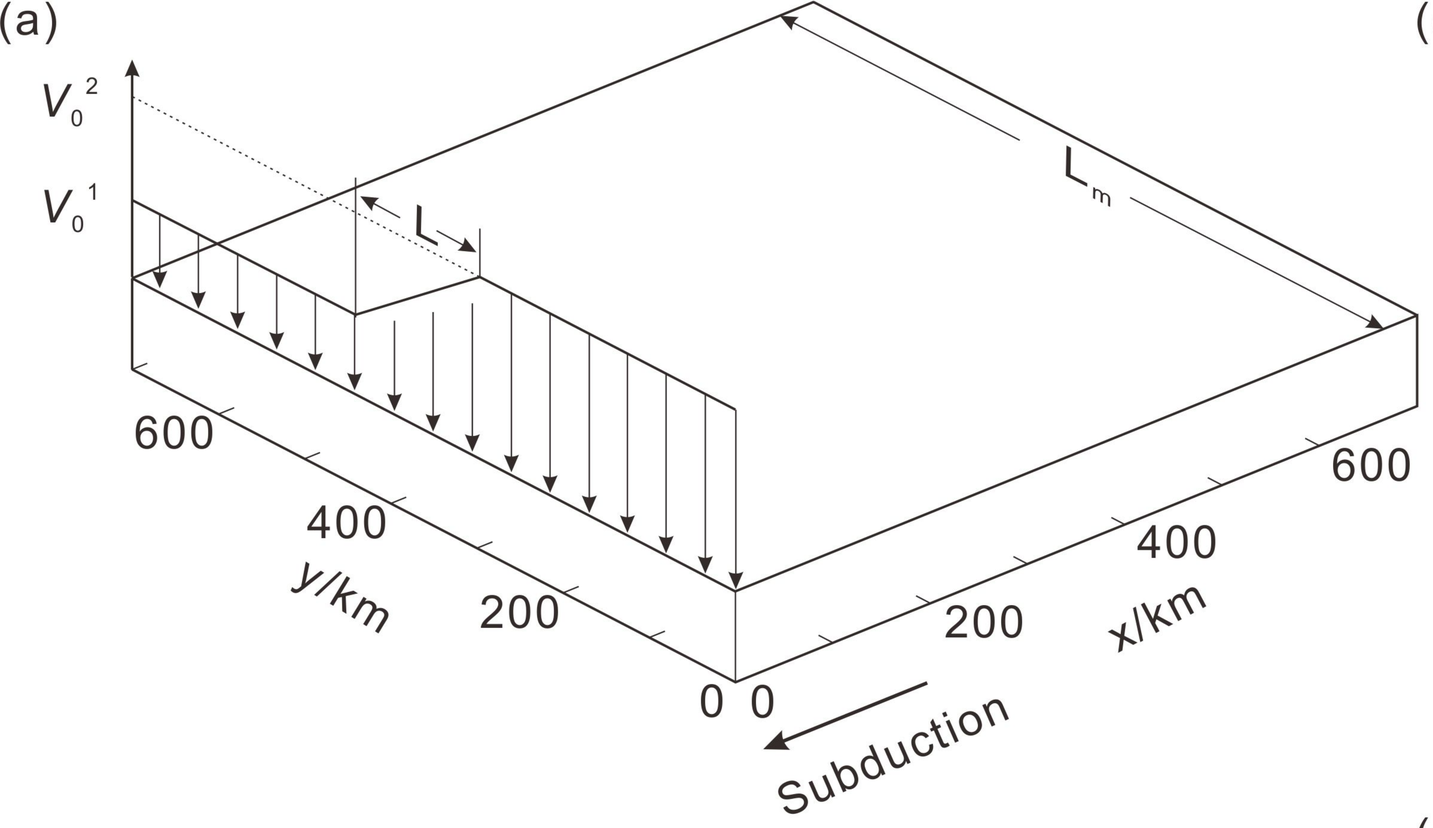
V_0^2
V_0^1
L
L_m
600
400
y/km
200
0
0
200
400
x/km
600
Subduction

(b)

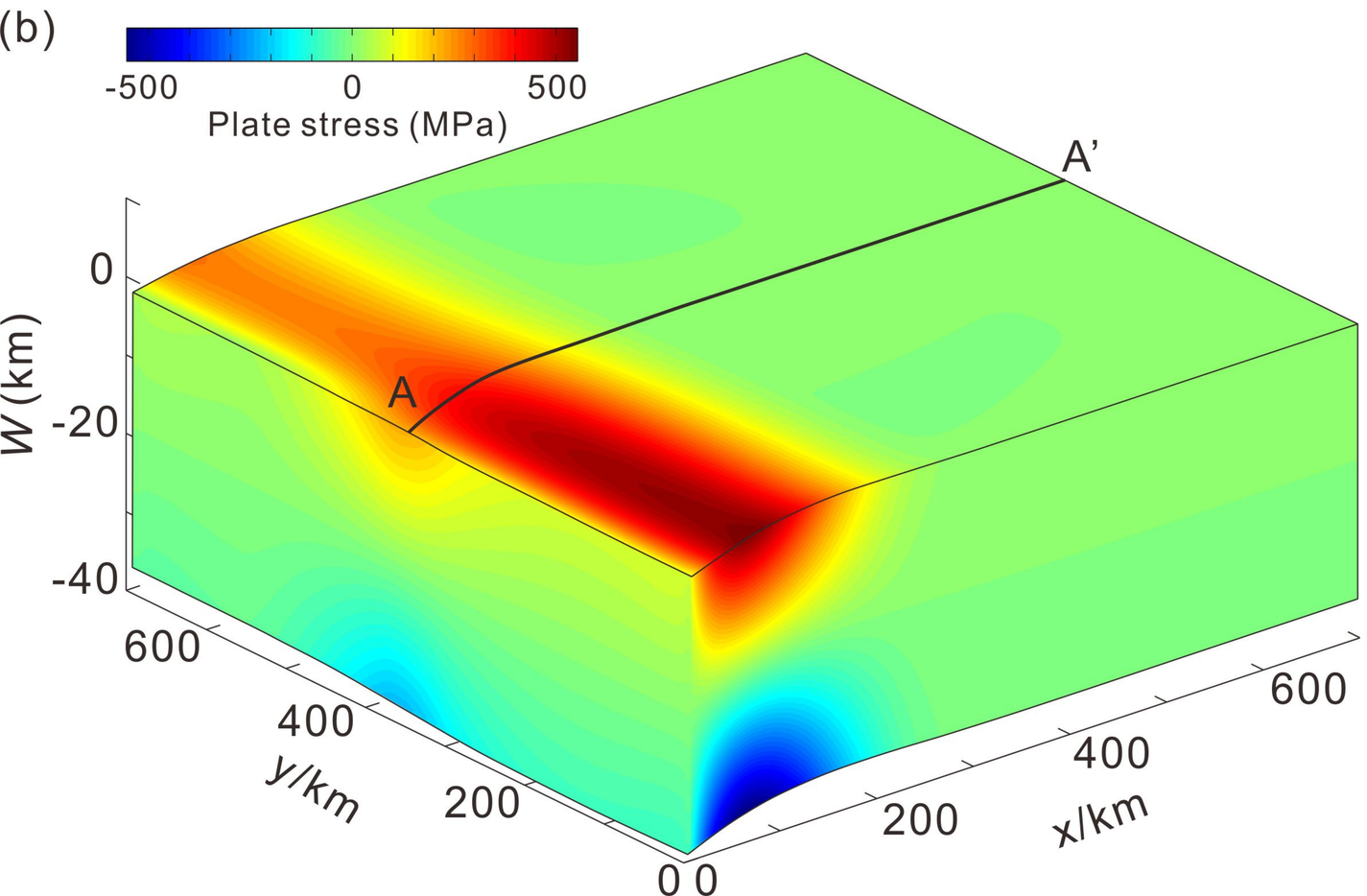
-500
0
500
Plate stress (MPa)
A'
A
0
-20
-40
W (km)
600
400
y/km
200
0
0
200
400
x/km
600

(c)

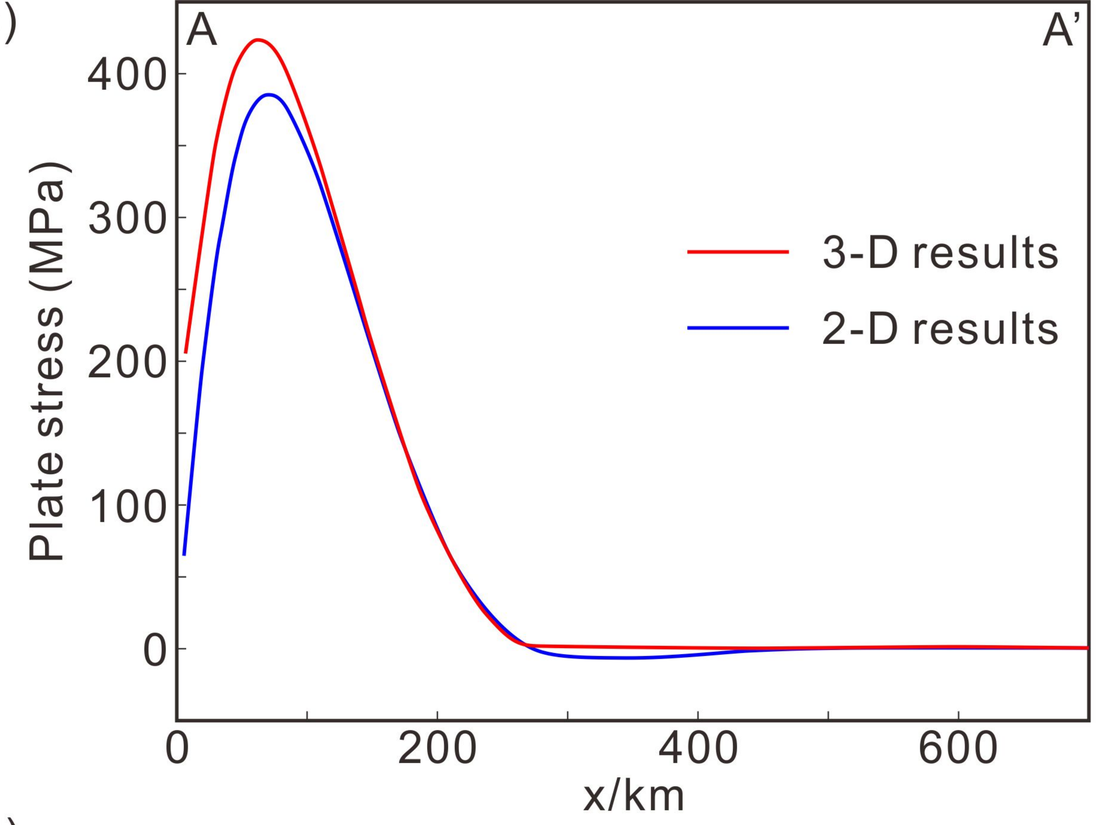
A
A'
400
300
200
100
0
Plate stress (MPa)
3-D results
2-D results
0
200
400
600
x/km

(d)

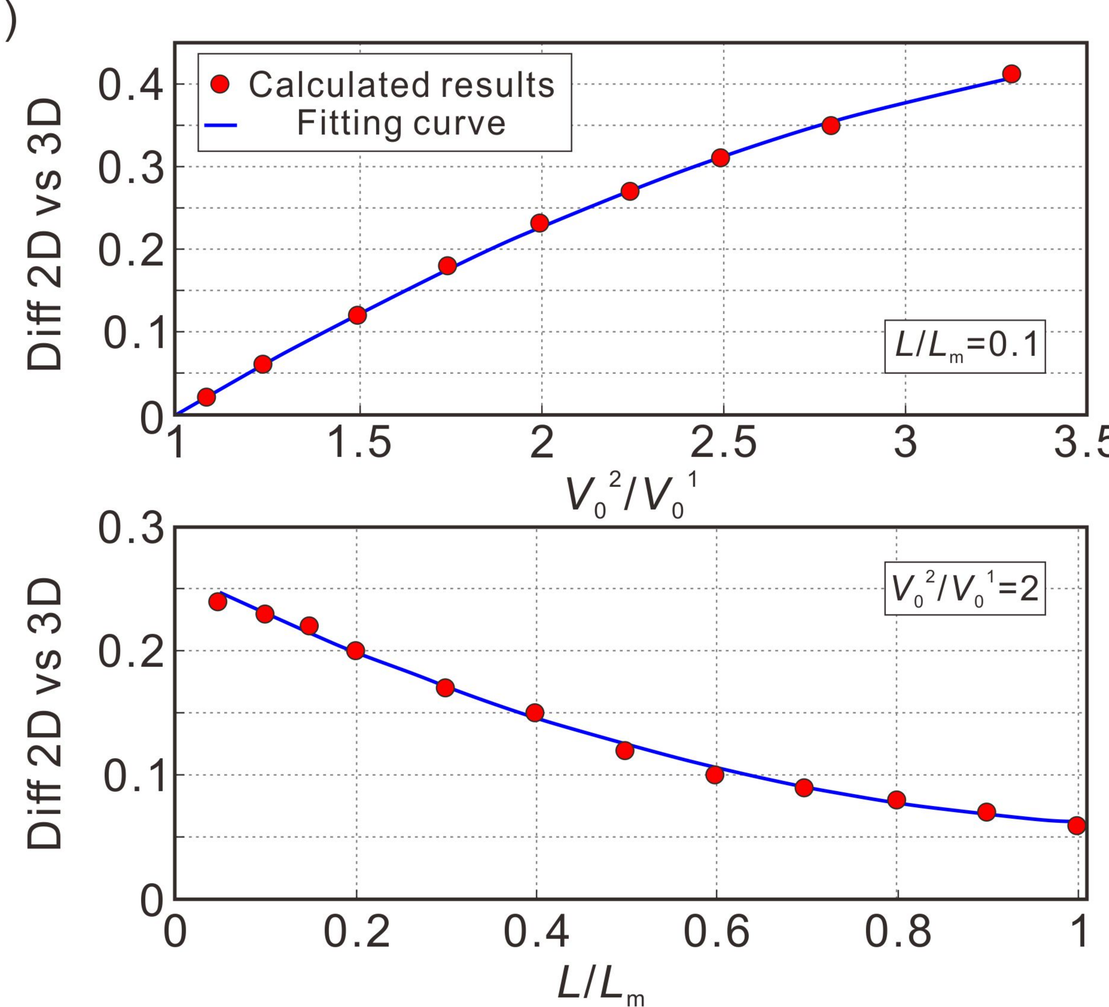
Calculated results
Fitting curve
L/L_m=0.1
Diff 2D vs 3D
0.4
0.3
0.2
0.1
0
1
1.5
2
2.5
3
3.5
V_0^2/V_0^1
V_0^2/V_0^1=2
Diff 2D vs 3D
0.3
0.2
0.1
0
0
0.2
0.4
0.6
0.8
1
L/L_m

Figure05.

(a)

Location of the stress profile in (b)

Depth (km)

0
20
40
60

300
200
y(km)
100
0

0
100
200
300
x(km)

-2000 -1000 0 1000 2000 (Mpa)

(b)

Compression

Extension

0
10
20
30
40
50
60

Depth (km)

Byerlee (1978)

Mei et al. (2010)

κ=5.8x10^{-7}

T_e^M~50km

Age ~150Ma

Neutral Plane
~25 km

d_y

σ^e

Elastic core

Hirth & Kohlstedt (2003)

Mechanical Thickness
~59.4 km

-1500 -1000 -500 0 500 1000 1500

Stress (MPa)

Lateral change of in-plate stress and seismicity along the southern Mariana trench

Jiangyang Zhang[1, 2], Hongfeng Yang[2, 1]*, Han Chen[2], Fan Zhang[3], Gaohua Zhu[2], and Zhen Sun[3]

[1]. *Shenzhen Research Institute, The Chinese University of Hong Kong, Shenzhen, 518057, China*

[2]. *Earth System Science Programme, The Chinese University of Hong Kong, Shatin, NT, Hong Kong, China.*

[3]. *CAS Key Laboratory of Ocean and Marginal Sea Geology, Chinese Academy of Sciences, South China Sea Institute of Oceanology, Guangzhou 510301, China.*

* Corresponding author, Hongfeng Yang (hyang@cuhk.edu.hk)

Abstract

Lithospheric flexure at subduction zones is a major contributor to induce outer rise earthquakes. Here, we modeled the bending deformation of the subducting plate at the southern Mariana using a 3-D plate flexural model. Intraplate stresses were investigated, with the along-strike variable boundary loadings. In order to match the observations of plate geometry, boundary vertical loading near the Challenger Deep has to be set twice of that in other areas. We also compared results between 2-D and 3-D models and found that the difference on estimating plate stress can exceed 20% when there is an along-strike variation in plate bending. Finally, we found that the sharp lateral variation in

the σ^{e}_{yy} and the σ^{e}_{xy} corresponded to an outer rise earthquake cluster at the southern Mariana subduction zone, indicating that along-strike variation in σ^{e}_{yy} and σ^{e}_{xy} may be a significant mechanism to cause non-uniform distribution of outer rise earthquakes.

Plain Language Summary

A subduction zone is a region where two tectonic plates converged. When a plate is subducted beneath the other one and becomes bending, the accumulation of bending stress will occur. If the bending stress exceeds the yield strength of lithosphere, it will induce the normal faults and earthquakes at outer rise. In our study, we simulated the bending deformation of subducted plate at the southern Mariana subduction zone and calculated corresponding stresses using the 3-D plate bending model. We found that there is difference between the 2-D and 3-D model on estimating plate bending stress when there is an along-strike variation of plate bending. We further found that the plate bending stress has very important relationship with the distribution of outer rise earthquakes.

Key words: Mariana Subduction zone; Plate bending; Numerical simulation; Stress; Earthquakes

1. Introduction

Widely distributed subduction zone earthquakes may trigger large tsunami and cause significant loss of life and damage, as demonstrated by numerous examples (e.g. Gusman et al., 2009; Lay et al., 2010). In addition to interplate earthquakes, there are intra-plate earthquakes which could also be devastating, such as the 1977 Sumba

Indonesia (Sunda trench, M_w=8.3) (Lynnes and Lay, 1988), the 1990 Mariana Trench (M_w=7.3) (Yoshida et al., 1992), the 2007 Kuril Trench (M_w=8.1) (Ammon et al., 2008), and the 2009 Somoa-Tonga (M_w=8.1, Beavan et al., 2010; Lay et al., 2010) earthquakes. All of these earthquakes occurred in the outer rise region seaward of trench in subduction zones, where normal faults are generated or reactivated by plate bending (Mortera-Gutiérrez et al., 2003; Ranero et al., 2003; 2005). An outer rise earthquake may be triggered by a megathrust earthquake and sometimes may trigger a megathrust event (Ammon et al., 2008; Beavan et al., 2010; Lay et al., 2010), enhancing the tsunami hazard potential. Therefore, evaluating plate bending, stress distribution, and corresponding earthquakes in the outer rise region are crucial to assess earthquake and tsunami hazard in subduction zones.

Previous studies have recognized the important role of stress within the subducting plate in outer rise earthquakes (Chapple and Forsyth, 1979; Christensen and Ruff, 1983, 1988; Scholz and Small, 1995; Emry et al., 2014; Zhou et al., 2015, 2018). For instance, Chapple and Forsyth (1979) explained the depths of tensional and compressional outer rise earthquakes by using the idea that plate bending can produce tensional and compressional stress regime, separated by a neutral plane. This model was supported by focal mechanism solutions of outer rise earthquakes, e.g. along the Mariana subduction zone where the focal depths of normal faulting events delineate the boundary between the extension and compression stress regimes (Emry et al., 2014). Zhang et al., (2014) simulated the geometry of the subducted plate along the profile perpendicular to the Mariana Trench using a two-segment effective elastic thickness (T_e) flexural model. They

64 suggested that the plate bending stresses could exceed the lithosphere yield strength
65 envelope (YSE) resulting in faulting and tensional earthquakes in the upper plate,
66 corresponding to the reduction in T_e. Their results showed a 21-61% reduction in T_e along
67 the Mariana.

68 All of their work are based on 2-D flexural models, which only consider the bending
69 or slab pull from the direction perpendicular to the trench and assume uniform stress
70 along the trench. However, recent works clearly show along-strike variation in distribution
71 of outer rise seismicity, e.g. the southern Mariana subduction zone (Zhu et al., 2019)
72 where pervasive normal faults are observed (Figure 1). Moreover, observations of
73 strike-slip earthquakes in outer rise further indicate complex stress fields and thus require
74 investigations considering laterally varying boundary conditions and loadings, rather than
75 2-D plate bending models.

76 Some 3-D plate bending models have been developed to investigate the subducted
77 plate geometry (Manríquez et al., 2014) and boundary loading variation (Zhang et al.,
78 2018). However, no models have incorporated different aspects so as to provide
79 constraints on in-plate stress. Here we develop a 3D model by incorporating bathymetries
80 of the incoming plate, geometries of the subducting slab, and varying loading conditions.
81 We then apply this model in the southern Mariana subduction zone and derive stress
82 distribution within the incoming plate, for the first time. The distribution of surface elastic
83 stress is compared to the earthquake locations that were obtained from the recently
84 acquired seismic data (Zhu et al., 2019). In the end we discuss the possible relationship
85 between the plate bending, stress, and the distribution of outer rise normal fault

86 earthquakes.

87 **2. Data and method**

88 2.1. Data Preparation

89 Three kinds of data were used in our study, including 15 arc-second resolution
90 global bathymetry data (Olson et al., 2014) and local multibeam data with ~150m
91 resolution (data from the NOAA website: https://www.ngdc.noaa.gov/maps/autogrid/),
92 global slabs geometry data (Slab 2.0 from Hayes et al., 2018), and newly acquired ocean
93 bottom seismic data (Zhu et al., 2019). Firstly, we identified the strike of the
94 bending-related normal faults from the multibeam data, as did in Ranero et al. (2005) for
95 the Mid-America and the Chile Trench. Rose diagrams of the fault strike help us to
96 determine the bending direction of the plate (Figure1b and d). In order to make the plate
97 boundary parallel to the strike of normal fault, the model area was chosen following the
98 bending direction (red rectangle in the Figure 1a). Then, the bathymetry data and Slab2.0
99 data are stitched together to provide well constraints on 3-D plate bending models.

100 2.2. Flexure model and inversion

101 It is widely accepted that the lithospheric plate is regarded as an elastic layer
102 floating on an inviscid layer and the flexure deformation can therefore be modeled by an
103 elastic thin plate under applied external forces (Watts, 2001; Turcotte and Schubert, 2014).
104 At subduction zones, if the strong plate bending exceeds the lithospheric yield strength, it
105 can result in bending-related normal faults, earthquakes and mantle serpentinization near

106 the outer rise(Grevemeyeretal.2005; Ranero et al. 2005). This process may result in the
107 loss of strength and flexural rigidity of the lithosphere (Contreras-Reyes and Osses, 2010).
108 A plate bending model with variable flexural rigidity was therefore usually used to model
109 the deformation of the subducted plate (Zhang et al., 2014; Hunter and Watts, 2016;
110 Zhang et al., 2018).

111 The flexure model and inversion method used in this paper are similar to Zhang et
112 al., (2018). The plate deflection *w* was inverted by solving the 3-D plate flexure equation
113 with the finite difference method (FDM), as well as the Particle Swarm Optimization (PSO)
114 inversion method. The details of methodology have been described in Zhang et al., (2019).
115 For simplicity, the T_e was divided into two parts (T_e^M and T_e^m) in our model similar to
116 previous studies (Contreras-Reyes and Osses, 2010; Zhang et al., 2014). The T_e^M
117 represents the seaward T_e where the curvature of plate is zero (Contreras-Reyes and
118 Osses, 2010) and the T_e^m stands for landward T_e deduced by normal faults and
119 serpentinization. Previous studies showed that the T_e of the oceanic plate at subduction
120 zone depends on plate age (Zhang et al., 2018). The age of subducting plate at southern
121 Mariana subduction zone ranges from 145 to 150 MPa (Figure 1a and b), the T_e^M is
122 therefore set to a constant (50km) in our model.

123 The calculated area is set to a rectangle with *x* axis perpendicular to the trench and
124 *y* axis along the trench (Figure 1d). The trench axis was set to be ~100km away from the
125 boundary and the part landward of the trench was constrained by Slab2.0. Because the
126 direction of trench strike is variable, if the curved trench was set to be the loading
127 boundary, it may not be reflective of the bending direction of plate (Figure 1d). Choosing

the deep slab as the boundary has at least two advantages. One is that it keeps the outer rise area away from the boundary, so the boundary effect can be avoided. The other one is that it can help us handle the effect caused by the local topographic reliefs (such as seamounts) better, because our aim is to model the first-order deformation of the subducting plate and the local topographic reliefs are noise that should be removed in our simulation. Both bending moment (M_0) and vertical shear force (V_0) vary along the boundary. The squared RMS (root mean square) error W_{rms} between the observed data and the modeled flexure is used to find the best-fit model.

2.3. In-plate stresses distribution

For the thin elastic plates, the components of the plane stress along the *x* and *y* axis depending on the distance from the neutral plane (*z*) are given by:

$$\begin{bmatrix} \sigma_{xx} \\ \sigma_{yy} \\ \tau_{xy} \end{bmatrix} = -\frac{Ez}{1+\mu} \begin{bmatrix} \frac{1}{1-\mu} & \frac{\mu}{1-\mu} & 0 \\ \frac{\mu}{1-\mu} & \frac{1}{1-\mu} & 0 \\ 0 & 0 & 1 \end{bmatrix} \begin{bmatrix} \frac{\partial^2 w}{\partial x^2} \\ \frac{\partial^2 w}{\partial y^2} \\ \frac{\partial^2 w}{\partial x \partial y} \end{bmatrix} \quad (1)$$

where *E* and *μ* represent the Young's modulus and the Poisson's ratio which are set to 7 $\times 10^{10}$ Pa and 0.25 respectively. When we discuss the elastic core and the depth of plastic deformation constrained by the YSE, these stress components need to be projected onto the principal stress axes by:

$$\sigma_1 = \frac{\sigma_{xx} + \sigma_{yy}}{2} + \sqrt{\left(\frac{\sigma_{xx} - \sigma_{yy}}{2}\right)^2 + \tau_{xy}{}^2}$$
$$\sigma_2 = \frac{\sigma_{xx} + \sigma_{yy}}{2} - \sqrt{\left(\frac{\sigma_{xx} - \sigma_{yy}}{2}\right)^2 + \tau_{xy}{}^2} \quad (2)$$

3. Results

3.1. Statistics of fault strike at outer rise

In the southern Mariana, the magnetic lineation is obvious oblique to the trench and the bending normal faults. So it is suggested that the bending normal faults in the southern Mariana have no clear relationship with spreading. We identified ~260 bending faults from the multibeam bathymetry data using the method similar to Ranero et al., 2005 (Figure 1b and c). The rose diagram shows that the main direction of the fault strike is NEE (Figure 1c) and thus the green arrow shows that the bending direction is NNW. These two directions help us to determine the geographical range of our model (Figure 1).

3.2. Plate bending

A series of numerical model have been performed for a range of boundary loadings and plate effective thickness. Finally we choose the best-fitting model with the W_{rms} less than 1.5 km. We obtained smooth model results, including the 3-D simulated plate deformation (Figure 2b) and different profiles (Figure 2c-f). The red lines show the results of our model and the black lines are observed data. Profiles perpendicular to the trench showed a ~1 km deviation between observations and our modeling results within 0 to 100km (Figure 2c and d). This may be caused by the discontinuity of the two datasets as the precision of Slab2.0 is much lower than that of bathymetry. However, we believe that this deviation would not affect the accuracy of our model, because the scale of our model is far greater than ~1km.

Along the strike of the trench, we found that the flexural depth of the subducted

166 plate becomes deeper from east to west, with a sharp variation of depth at the ~150km
167 along the trench axis (Figure 2a, b and e). Such along-strike variation may be associated
168 with the deepest spot, Challenger Deep (Figure 2f). To match the plate deformation,
169 along-strike variable loadings were applied on the plate boundary. The bending moment
170 applied on the western part (near the Challenger Deep) is nearly twice as much as that of
171 the eastern part.

172 3.3. Stresses and earthquakes distribution

173 According to equations (1) and (2), the distribution of surface elastic stress
174 components σ^e_{xx}, σ^e_{yy}, σ^e_{xy} and the maximum principal stress σ^e_1 are calculated in the
175 best-fitting model (Figure 3). The σ^e_{xx} stands for the normal stress along the *x* axis (the
176 direction perpendicular to the trench) caused by plate bending perpendicular to the trench
177 and it reaches maximum close to the trench axis. The σ^e_{yy} represents the normal stress
178 along the strike of the trench mainly caused by lateral flexural deformation of the plate (the
179 direction along the trench). This means if the flexure morphology of the plate is invariant
180 along the strike of the trench, the σ^e_{yy} will present the same tendency with σ^e_{xx} due to the
181 Poisson's ratio of materials. Conversely, if the flexure morphology of plate varies along the
182 strike of the trench, the σ^e_{yy} will change due to the lateral plate pull. The σ^e_{xy} represents
183 the shear force also caused by the lateral plate pull. If no lateral plate pulling exists, the
184 σ^e_{xy} will be zero.

185 We found that the stress distribution associated with the plate bending is
186 heterogeneous. In addition, the σ^e_{xx} increases gradually from the outer rise to the trench

and reaches the maximum at the Challenger Deep, consistent with previous studies (Zhang et al., 2014, 2019). The σ^{e}_{xy} variations from extension to compression (or the opposite) and The σ^{e}_{yy} shows a high value at ~143° E, 11-11.5°N. Among the stress components, the σ^{e}_{xx} is the largest, reaching the maximum of ~5GPa. The maximum of σ^{e}_{1} exceeds 6GPa. Along the red line in Figure 3d, the depth of earthquakes and the variation of σ^{e}_{1} were projected onto the profile in Figure 3e. It shows that from west to east, there is a sudden drop of the σ^{e}_{1} at the distance ~40 - 60km (please note the stress axis is reversed) and most of the earthquakes occur at this area. The depths of the earthquakes vary from 0 to ~60km with the mode number of depth ~26km (the histogram in Figure 3e).

4. Discussion

4.1. Comparison between the 2-D and the 3-D model on estimating the plate stress

The stress distribution of the flexural lithosphere could be predicted by the curvature of the 2-D profile perpendicular to the trench (Hunter et al., 2016; Zhang et al., 2019). The plate stress distribution can further help us constrain the lithospheric yield zone, the depth of outer rise earthquakes and mantle serpentinization (Emry et al., 2014; Zhang et al., 2019). Garcia et al. (2019) suggested that the amount of strain ε (as well as the stress σ) of a flexural plate can be described by: $\varepsilon = -z\frac{\partial^2 w}{\partial x'^2}$, where x' is a horizontal coordinate axis along the direction of maximum curvature. If the flexural parameters (such as M_0 and V_0) are invariant along trench, the direction of maximum curvature is perpendicular to the trench and the plate stress estimated by the 2-D model is nearly equal to that estimated

by the 3-D model. However, if the flexural parameters vary along trench, the direction of maximum curvature will change and point to the lowest place of the three-dimensional space. At this situation, the plate stress estimated by the 2-D profile curvature may be underestimated.

Figure 4 is an example that illustrates how along-strike variable V_0 generates the underestimated 2-D plate stress. Here, the V_0 is set to sectioned linear variation along the strike, which means that the V_0 change from V_0^1 to V_0^2 linearly within a variation distance L (Figure 4a). As we only consider the effects of the along-strike variable V_0, the T_e was set to a constant value (35km) here. Then we compared the difference between the 2-D and the 3-D model on estimating plate stress (Figure 4c). After employing dozens of different calculation models, we found that both the change in V_0 and the variation distance L (we used L/L_m in Figure 4d, where Lm is the width of our model) can affect the difference between the 2-D and the 3-D model. It shows that the difference between the 2-D and 3-D the model on estimating plate stress increases with change of V_0 and decrease with the variation distance L (Figure 4d). Considering the Mariana Trench, if the L/L_m equals to 0.1 and V_0^2/V_0^1 is set to 2, the difference between the 2-D and the 3-D model can exceed 20% (Figure 4).

4.2. Surface elastic stress and the YSE

The in-plate stress of the elastic plate is linearly correlated with the distance from the neutral plane of the plate (z) (Equation 1). It means that the stress varies linearly from the maximum compressive stress to the Maximum tensile stress along the traversal

section of a bending plate. However, the lithosphere is not perfect elastic. It will be yield and generate plastic deformation (such as normal fault) when the stress exceeds the yield strength of the lithosphere.

The stress distributions along different profiles at the South Mariana Trench in our model are shown in Figure 5a. If the subducted plate is the ideal pure elastic material, the surface elastic stress can reach ~3GPa. While the actual plate bending stress is of limited by the YSE. The YSE used in our study is combination of Beyerlee (1978), Mei et al. (2010) and Hirth and Kohlstedt (2003) (Figure 5b). In Figure 5b, the grey line represents the elastic stress profile at the location pointed by the red arrow in Figure 5a. σ^e is the surface elastic stress and d_y is the depth of the yield zone. Clearly, the d_y is linearly positively correlated to the σ^e. It means that if the σ^e is given at anyplace, the d_y can be estimated easily. Therefore, we can use the simulated surface elastic stress to constraint the potential first fracture zone and the distribution of outer rise earthquakes.

4.3. Lateral variation of in-plate stress and outer rise earthquakes

Along the strike of the Mariana trench, the distribution of outer rise earthquakes is always non-uniform (Zhu et al., 2019). Christensen and Ruff (1988) proposed a model by considering the regional and plate bending stress to explain such phenomena. They indicated that although the lithospheric bending played a major role in inducing outer rise tensional earthquakes by placing the shallow region of outer rise in extension and causing brittle deformation, the regional compressional stress caused by the interaction between the upper and subducted plate can reduce the possibility of outer rise extensional events,

such as the alternation of tensional and compressional outer rise earthquakes along the Kuril subduction zone (Ammon et al., 2008). However, previous studies have demonstrated a weak plate coupling at the southernmost Mariana Trench (Gvirtzman and Stern, 2004; Emry et al., 2014). It is unlikely that the uneven distribution of outer rise earthquakes located by Zhu et al., (2019) can be explained by the coupling between the upper and subducted plates.

Here, we proposed another possible mechanism which causes the variable distribution of outer rise earthquakes - the lateral variation of in-plate stress. If there is a variable boundary loading caused by deep slab pull, it will lead to the along-strike variable bending depth as well as the variable plate bending stress at outer rise. We propose that the bending stresses exceed the yield strength of the lithosphere due to the variable loading, corresponding to the variable distribution of outer rise seismicity. Here the bending stress includes not only the stress along the direction perpendicular to the trench but also the stress along the strike of the trench (σ^{e}_{yy} and σ^{e}_{xy}) caused by the laterally plate pull. Actually, we found that the along-strike stress plays an unneglectable role in deciding the distribution of outer rise earthquakes. For example at the southern Mariana Trench, it is hard to explain the concentrated outer rise seismicity only by the extensional stress along the direction perpendicular to the trench. However, a sharp variation of the normal stress along the strike of the trench (σ^{e}_{yy}) occurred just at the concentrated seismic zone (Figure 3b).

5. Conclusion

By analyzing the results of plate bending simulation, in-plate stress, and the distribution of outer rise earthquakes, we show that the variable boundary loadings along the strike of southern Mariana Trench caused by deep slab pull can cause not only along-strike variation in degree of plate bending, but also the along-strike variant in-plate stresses. The boundary loading applied at the Challenger Deep area is nearly twice as much as that of other areas, which can make the difference between the 2-D and the 3-D model on estimating the plate stress exceed 20%. An outer rise zone with concentrated earthquakes in the southern Mariana subduction zone corresponds to the sharp variation in the along-strike normal stress and the plane shear stress. It is therefore suggested that the 3-D effect of plate bending can be a mechanism to cause non-uniform distribution of outer rise earthquakes along trench.

6. Acknowledgements

We are grateful to Prof. Jian Lin, Dr. Xiaohuan Jiang, Xiang Chen, Suli Yao, Pengcheng Zhou and Junhao Song for useful discussion. We thank Zhongxian Zhao and Zhiyuan Zhou for offering technical assistance. GMT (Wessel and Smith 1995) was used to draw the topographic map. The bathymetry data can be found at the website: https://catalog.data.gov/dataset/srtm15-plus-estimated-topography-15-seconds-global-v1. The multibeam data with ~150m resolution can be found at the NOAA website: https://www.ngdc.noaa.gov/maps/autogrid/ and the global slabs geometry data Slab 2.0 can be found at https://www.sciencebase.gov/catalog/item/5aa1b00ee4b0b1c392e86467

(Hayes et al., 2018).

This research is supported by National Key R&D Program of China (Grant Number 2018YFC1503400), Hong Kong Research Grant Council Grants (No. 14313816), Faculty of Science at CUHK, China Postdoctoral Science Foundation (No. 2019M663119), the Guangdong NSF research team project (2017A030312002), and the National Science Foundation of China (No. 41976064).

Reference

Ammon, C.J., Kanamori, H., Lay, T., 2008. A great earthquake doublet and seismic stress transfer cycle in the central Kuril islands. Nature 451, 561-566.

Beaven, J., Wang, X., Holden, C., Wilson, K., Power, W., Prasetya, G., Bevis, M., Kautoke, R., 2010. Near-simultaneous great earthquakes at Tongan megathrust and outer rise in September 2009. Nature 466, 959-963

Byerlee, J., 1978. Friction of rocks. Pure appl. Geophys. 116 (4-5), 615-626.

Chapple, W.M., Forsyth, D.W., 1979. Earthquakes and bending of plates at trenches. J. Geophys. Res. 84 (B12), 6729-6749.

Christensen, D.H., Ruff, L.J., 1983. Outer-rise earthquakes and seismic coupling. Geophys. Res. Lett. 10, 697-700.

Christensen, D.H., Ruff, L.J., 1988. Seismic Coupling and Outer Rise Earthquakes. J. Geophys. Res. 93 (B11), 13,421-13,444.

Contreras-Reyes, E., Osses, A., 2010. Lithospheric flexure modelling seaward of the

311 Chile trench: implications for oceanic plate weakening in the Trench Outer Rise
312 region. Geophys. J. Int. 182 (1), 97-112.
313 Emry, E.L., Wiens, D.A., Garcia-Castellanos., 2014. Faulting within the Pacific plate at the
314 Mariana Trench: Implications for plate interface coupling and subduction of hydrous
315 minerals. J. Geophys. Res. Solid Earth 119, 2076-3095.
316 Garcia, E.S., Sandwell, D.T., Bassett, D., 2019. Outer Trench Slope Flexure and Faulting
317 at Pacific Basin Subduction Zones. Geophys. J. Int. DOI: 10.31223/osf.io/dbn8j.
318 Grevemeyer, I., Kaul, N., Diaz-Naveas, J.L., Villinger, H., Ranero, C.R., Reichert, C., 2005.
319 Heat flow and bending-related faulting at subduction trenches: Case studies offshore
320 of Nicaragua and Central Chile. Earth planet. Sci. Lett. 236, 238-248.
321 Gusman, A.R., Tanioka, Y., Matsumoto, H., Iwasaki, S-I., 2009. Analysis of the Tsunami
322 Generated by the Great 1977 Sumba Earthquake that Occurred in Indonesia. Bull.
323 Seismol. Soc. Am. 99 (4), 2169-2179.
324 Gvirtzman, Z., Stern, R.J., 2004. Bathymetry of Mariana trench-arc system and formation
325 of the Challenger Deep as a consequence of weak plate coupling. Tectonics 23,
326 TC2011.
327 Hayes, G., 2018, Slab2 - A Comprehensive Subduction Zone Geometry Model: U.S.
328 Geological Survey data release, https://doi.org/10.5066/F7PV6JNV.
329 Hirth, G., Kohlstedt, D., 2003. Rheology of the Upper Mantle and the Mantle Wedge: A
330 View from the Experimentalists. in *Inside the Subduction Factory*, pp. 83-105, ed.
331 Eiler, J., American Geophysical Union.
332 Hunter, J., Watts, A.B., 2016. Gravity anomalies, flexure and mantle rheology seaward of

circum-Pacific trenches. Geophys. J. Int. 207 (1), 288-316.

Lay, T., Ammon, C. J., Kanamori, H., Rivera, L., Koper, K. D., Hutko, A. R., 2010. The 2009 Samoa-Tonga great earthquake triggered doublet. Nature 466, 964–967.

Lay, T., Ye, L., Bai, Y., Cheung, K.F., Kanamori, H., 2018. The 2018 M_W 7.9 Gulf of Alaska Earthquake: Multiple Fault Rupture in the Pacific Plate. Geophys. Res. Lett. 45, 9542–9551.

Lynnes, C., Lay, T., 1988. Source process of the great Sumba earthquake. J. Geophys. Res. 93, 13,407-14,320.

Manríquez, P., Contreras-Reyes, E., Osses, A., 2014. Lithospheric 3-D flexure modelling of the oceanic plate seaward of the trench using variable elastic thickness. Geophys. J. Int. 196, 681–693.

Mei, S., Suzuki, A.M., Kohlstedt, D.L., Dixon, N.A., Durham, W.B., 2010. Experimental constraints on the strength of the lithospheric mantle. J. Geophys. Res. 115 (B8).

Mortera-Gutiérrez, C.A., Scholl, D.W., Carlson, R.L., 2003. Fault trends on the seaward slope of the Aleutian Trench: Implications for a laterally changing stress field tied to a westward increase in oblique convergence. J. Geophys. Res. 108, 2477.

Ranero, C.R., Morgan, J.P., McIntosh, K., Reichert, C., 2003. Bending-related faulting and mantle serpentinization at the Middle America trench. Nature 425(6956), 367–373.

Ranero, C.R., Villaseñor, A., Morgan, J.P., Weinrebe, W., 2005. Relationship between bending-faulting at trenches and intermediate-depth seismicity. Geochem. Geophys. Geosyst. 6 (12).

Scholz, C. H., Campos, J., 1995. On the mechanism of seismic decoupling and back arc

spreading at subduction zones, J. Geophys. Res., 100 (B11), 22,103–22,115.

Turcotte, D., Schubert, G., 2014. *Geodynamics*, 3nd edn. Cambridge University Press, pp. 626.

Watts, A.B., 2001. *Isostasy and Flexure of the Lithosphere*, 1st edn, Cambridge University Press, New York, pp. 478.

Yoshida, Y., Satake, K., Abe, K., 1992. The large normal-faulting Mariana Earthquake of April 5, 1990 in uncoupled subduction zone. Geophys. Res. Lett. 19 (3), 297-300.

Zhang, F., Lin, J., Zhan, W., 2014. Variations in oceanic plate bending along the Mariana trench. Earth planet. Sci. Lett. 401, 206-214.

Zhang, F., Lin, J., Zhou, Z., Yang, H., Zhan W., 2018a. Intra- and intertrench variations in flexural bending of the Manila, Mariana and global trenches: implications on plate weakening in controlling trench dynamics. Geophys. J. Int. 212, 1429-1449.

Zhang, J., Sun, Z., Qiu, N., Zhang, Y., Li, F., 2019. 3-D effective elastic thickness inversion of subduction zone based on particle swarm optimization algorithm. Chinese J. Geophys. (in Chinese) 62 (12), 4738-4749.

Zhang, J., Sun, Z., Xu, M., Yang, H., Zhang, Y., Li, F., 2018. Lithospheric 3-D flexural modelling of subducted oceanic plate with variable effective elastic thickness along the Manila Trench. Geophys. J. Int. 215, 2071-2092.

Zhou, Z., Lin, J., Behn, M.D., Olive, J.A., 2015. Mechanism for normal faulting in the subducting plate at the Mariana Trench. Geophys. Res. Lett. 42, 4309-4317.

Zhou, Z., Lin, J., Elasto-plastic deformation and plate weakening due to normal faulting in the subducting plate along the Mariana Trench. Tectonophysics 734, 59-68.

Zhu, G., Yang, H., Lin, J., Zhou, Z., Xu, M., Sun, J., Wan, K., 2019. Along-strike variation in slab geometry at the southern Mariana subduction zone revealed by seismicity through ocean bottom seismic experiments. Geophys. J. Int. 218 (3), 2122-2135.

Figures

Figure 1. (a) Seafloor bathymetry of the southern Mariana Trench. The red rectangle is the domain of our 3-D flexural model; the black square box is the area where the normal faults are identified with the multi-beam data (please see Figure 1b) and the yellow star represents the location of the Challenger Deep. Yellow lines are the magnetic lineation based on Zhou et al., (2015). (b) Tectonic structure of the oceanic plate. Red lines are normal faults identified from the multibeam. (c) The rose diagram (red part) shows that the direction of strike of the bending-normal faults is NEE at the southern Marina Trench and the green arrow perpendicular to the fault strike shows that the bending direction is NNW. (d) Schematic 3-D model to illustrate the bending stresses of subducted plate under along-strike variable loadings (bending moment (M_0) and vertical shear force (V_0) caused by deep slab pull). σ_{xx} and σ_{yy} represent the stresses on vertical profiles. σ^e_{xx}, σ^e_{yy}, and σ^e_{xy} are surface elastic stresses (The meaning of surface elastic stress is shown in Figure 6).

Figure 2. Result of our model. (a) Observed plate bending of the study area. (b) 3-D plate bending model results. Pro. A, B, C, and D represent the profiles shown in Fig 2c-f. The

398 Pro. D is along the trench axis. (c)-(f) Comparisons between our model and observed data
399 along different profiles in Figure 2(b).
400
401 Figure 3. The components of the surface elastic stress (the meaning of the surface elastic
402 stress is shown in Figure 5). The white circles represent the location of outer rise
403 earthquakes proposed by Zhu et al., (2019) and the grey crossing in Figure (a) are historic
404 outer rise earthquakes in this area (from USGS). (a) The distribution of σ^{e}_{xx}, the normal
405 stress along the direction perpendicular to the trench. The yellow star stands for the
406 location of the Challenger Deep. (b) The distribution of σ^{e}_{yy}, the normal stress along the
407 strike of the trench, and (c) The distribution of the plane shear stress σ^{e}_{yy}. (d) The
408 distribution of the maximum principal stress σ^{e}_{1} (Please see the equation (2)). (e) The σ^{e}_{1}
409 and depth of outer rise earthquakes along the profile A-A' in Figure (d). It shows that the
410 sharp variation of the σ^{e}_{1} along the strike of trench corresponds well to the concentrated
411 seismic zone. The histogram represents the variation of seismic depths.
412
413 Figure 4. The difference between the 2-D and the 3-D model on estimating the plate
414 stress. (a) Schematic 3-D model to illustrate the along-strike variable V_0. L is the variation
415 distance of V_0 and L_m is the width of our model. (b) The 3-D plate stress distribution under
416 the loading shown in Figure a. The difference of the surface elastic stress between the
417 2-D and the 3-D model along the profile A-A' in Figure b. (d) Plotting difference between
418 the 2-D and the 3-D model on estimating plate stress versus the change of V_0 (V_0^2/V_0^1)
419 and the L/L_m

Figure 5. The relationship between the surface elastic stress and outer rise earthquakes. (a) Profiles with different direction along the southern Mariana and their bending stress distributions. The red arrow is the location of the profile shown in Figure (b). (b) The YSE used by Hunter and Watts (2016) which is a combination of the rheology laws of Byerlee (1978), Mei et al. (2010), and Hirth and Kohlstedt (2003). The plate age at the southern Mariana Trench is nearly 160 Ma with a mechanical thickness of ~59km. The grey line represents the plate elastic stress profile and the red line represents the real stress profile due to plastic deformation. The σ^e is the surface elastic stress (a theoretical value in the model) and the d_y is the yield depth. It is suggested that bending-related normal fault (earthquake) occurred shallower than this depth. It shows that the σ^e is positively correlated with the d_y and therefore the σ^e can be used to constrain the potential first fracture zone.